Published in final edited form as:
DNA Repair (Amst). 2008 August 2; 7(8): 1340–1351. doi:10.1016/j.dnarep.2008.04.018.

A comparison of BRCT domains involved in nonhomologous end-joining: Introducing the solution structure of the BRCT domain of polymerase lambda

Geoffrey A. Mueller[1,§*], **Andrea F. Moon**[1,§], **Eugene F. DeRose**[1], **Jody M. Havener**[2], **Dale A. Ramsden**[2], **Lars C. Pedersen**[1], and **Robert E. London**[1]

1*Laboratory of Structural Biology, National Institute of Environmental Health Sciences. 111 T.W. Alexander Drive, MD MR-01, Research Triangle Park, North Carolina 27709.*

2*Department of Biochemistry and Biophysics, University of North Carolina, Chapel Hill, NC 27599.*

Abstract

Three of the four family X polymerases, DNA polymerase λ, DNA polymerase μ, and TdT have been associated with repair of double-strand DNA breaks by nonhomologous end-joining. Their involvement in this DNA repair process requires an N-terminal BRCT domain that mediates interaction with other protein factors required for recognition and binding of broken DNA ends. Here we present the NMR solution structure of the BRCT domain of DNA polymerase λ, completing the structural portrait for this family of enzymes. Analysis of the overall fold of the polymerase λ BRCT domain reveals structural similarity to the BRCT domains of polymerase μ and TdT, yet highlights some key sequence and structural differences that may account for important differences in the biological activities of these enzymes and their roles in nonhomologous end-joining. Mutagenesis studies indicate that the conserved Arg57 residue of Pol λ plays a more critical role for binding to the XRCC4-Ligase IV complex than its structural homolog in Pol μ, Arg43. In contrast, the hydrophobic Leu60 residue of Pol λ contributes less significantly to binding than the structurally homologous Phe46 residue of Pol μ. A third leucine residue involved in the binding and activity of Pol μ, is nonconservatively replaced by a glutamine in Pol λ (Gln64) and, based on binding and activity data, is apparently unimportant for Pol λ interactions with the NHEJ complex. In conclusion, both the structure of the Pol λ BRCT domain and its mode of interaction with the other components of the NHEJ complex significantly differ from the two previously studied homologs, Pol μ and TdT.

Keywords

Family X Polymerase; DNA polymerase λ; TdT; DNA polymerase μ; BRCT domain; protein-protein interaction; nonhomologous end-joining

*Corresponding author: Phone: 919-541-3872; Fax: 919-541-5707; Email: mueller3@niehs.nih.gov.
§These authors contributed equally.

The atomic coordinates for the ensemble of structures (PDB code 2JW5) have been deposited in the Protein Data Bank, Research Collaboratory for Structural Bioinformatics, Rutgers University, New Brunswick, NJ (http://www.rcsb.org).

Introduction

Although substantial progress has been made in the structural and biochemical characterization of Family X polymerases β (Pol β), Pol λ, Pol μ, and terminal deoxyribonucleotidyl transferase (TdT), our understanding of their physiological roles remains limited. Pol β and, to a certain extent Pol λ, are involved in recognition and resolution of single-stranded DNA breaks during base excision repair (BER) [1,2], while Pol λ, Pol μ, and TdT have been associated with nonhomologous end-joining (NHEJ), a pathway that resolves double strand breaks (DSBs) [3–6]. A combination of non-overlapping expression profiles and catalytic activities dictate distinct biological roles for Pol λ, Pol μ, and TdT in NHEJ. In that order, these polymerases possess both decreasing dependency on template [6], as well as increasingly restricted expression patterns [7,8]. For example, while Pol λ shows a template-dependency more similar to canonical polymerases and is widely expressed, TdT adds nucleotides preferentially in the absence of template, and is expressed only in lymphocytes active in V(D)J recombination.

Pol λ expression thus overlaps that of both Pol μ and TdT, but Pol λ's participation in NHEJ has a significantly different impact on how NHEJ repairs broken chromosomes. How, then, are the different polymerases selected in order to carry out their distinct biological roles? Family X polymerases λ, μ, and TdT each possess an N-terminal BRCT domain [9]which has an impact on their physiological activity. This BRCT domain allows all three polymerases to interact with the NHEJ factors Ku, XRCC4, and Ligase IV (reviewed in [10–12]), resulting in recruitment of the polymerases to the DNA ends. Deletion of the BRCT domain abolishes the ability of these polymerases to participate in NHEJ in certain contexts [4–6,13].

In order to understand the roles of these Family X polymerases in NHEJ and in other DNA repair processes, it is essential to characterize the structure of the BRCT domains and to elucidate the critical interaction factors that determine polymerase selection by the NHEJ complex. Solution structures of the BRCT domains of Pol μ (PDB codes 2DUN and 2HTF [14]) and TdT (PDB code 2COE) recently have been solved by NMR spectroscopy. These BRCT domains exhibit a high degree of sequence identity (44%) [14,15]), a result consistent with their comparable interactions with the Ku/XRCC4-LigaseIV complex. However, sequence comparisons between the BRCT domains show that Pol λ, exhibits the least sequence similarity (Pol λ vs. Pol μ 23%, Pol λ vs. TdT 20%). In order to determine whether the greater sequence variability corresponds to a more significant structural difference, or to residue variations within a highly conserved structure, we report here the solution structure of the Pol λ BRCT domain. This determination completes the structural portrait for the BRCT domains present within the Family X polymerases and provides insights into understanding the structural basis for both the similarities and variability that characterize how these polymerases interact with the other component proteins involved in NHEJ.

Materials and Methods

Expression and Purification of the Human Pol λ BRCT Domain

The coding sequence (residues Gly34-Pro135) of human Pol λ was cloned into the pGEX-4T3 bacterial expression vector (GE Healthcare) with a TEV protease cleavage site inserted upstream of the Pol λ coding sequence. The vector was transformed into *E. coli* BL21 Codon-Plus (DE3)-RP cells. The media utilized 100 μg/ml ampicillin and 35 μg/ml chloramphenicol for selection of the pGEX-4T3 vector and the Codon-Plus cells. The media was either LB medium, or M9 medium supplemented with BioExpress (Cambridge Isotope Labs) at 1:100 dilution, which we term 'M9+'. For isotopic labeling, $^{15}NH_4Cl$, ^{13}C-glucose, U-[^{15}N] BioExpress and U-[^{13}C,^{15}N] BioExpress were used in appropriate combination to produce either [^{15}N]- or [^{13}C, ^{15}N]-Pol λ BRCT domain. The Pol λ BRCT domain was purified by batch incubation of the soluble fraction with glutathione sepharose 4B resin, then cleaved from

the resin using TEV protease. Cleaved protein was concentrated to 10 mg/ml, and diluted to a final salt concentration of 75 mM NaCl using 25 mM Tris pH 7.5. The protein was further purified by affinity chromatography over a Mono Q HR 5/5 column (GE Healthcare). The Pol λ BRCT domain did not bind the column matrix, and eluted in the flowthrough fraction with high purity. The final buffer conditions were 25 mM Tris pH 7.5, 75 mM NaCl. The NMR buffer also contained 10 % D_2O for the deuterium lock.

^{15}N-labeled Pol λ BRCT was used to acquire the 3D ^{15}N-separated Nuclear Overhauser Enhancement Spectroscopy (NOESY) [16], ^{15}N-T_1, ^{15}N-T_2, [^{15}N, ^{1}H]-Nuclear Overhauser Enhancement (NOE) relaxation [17], Carr-Purcell Meiboom-Gill (CPMG) [18,19], and Residual Dipolar Coupling (RDC) experiments [20] with and without PF1 phage (Asla Biotech) [21]. The ^{13}C, ^{15}N-labeled Pol λ BRCT was used for all other experiments, including the 3D ^{13}C-separated NOESY [16].

Chemical Shift Assignments and Structure Calculation

The backbone resonances were assigned primarily through a combined analysis of the Heteronuclear Single Quantum Coherence (HSQC), HNCACB [22], and CBCACONH [23] using the RunAbout tool in NMRViewJ [24]. Aliphatic side chain assignments were made utilizing combinations of HNHA [25], H(CCO)NH, (H)CCONH, CCH-TOCSY, HCCH-TOCSY [26–29], and in rare cases, the NOE experiments. Aromatic side chains were assigned using the experiments of Yamazaki et al [30]. Data from all experiments were acquired on a Varian INOVA 500 MHz Spectrometer equipped with a cryogenically cooled probe. The only exception was the methyl-methyl NOESY [31], which was collected on a Varian INOVA 600 MHz Spectrometer, also with a cryogenically cooled probe to maximize the resolution.

Structure calculations utilized CYANA [32] to assign the NOEs and to calculate initial structures that were subsequently refined with XPLOR-NIH [33]. The input data to CYANA included the ^{15}N- and ^{13}C-separated NOESY experiments, dihedral bond angle restraints from TALOS [34], and the chemical shift assignments. Subsequent refinement with XPLOR-NIH of the best CYANA structure included the RDCs as restraints. Three rounds of refinement with XPLOR-NIH were utilized to filter a few problematic or frequently violated restraints, mostly in loop regions that were likely over-restrained by CYANA, which attempts to assign and calibrate all input peaks.

Activity and binding analysis of mutant proteins

N- and C-terminal hexahistidine tagged full-length Pol λ cDNA was generated by amplification and insertion between Nde I and Xho I sites of the bacterial expression vector pET28b (Novagen). The downstream amplification primer altered the reading frame starting at the second last amino acid, resulting in substitution of the terminal two amino acids (Asp574 and Trp575 to Thr and Gly, respectively) and allowing for an in frame translation of the vector-resident C-terminal hexahistidine tag. BRCT domain mutations were introduced in the context of this construct. Full-length constructs (wildtype and BRCT substitution mutations) were expressed and purified on a 1 ml HisTrap Fast-Flow Nickel column as previously described [14], and eluted in a buffer containing 25 mM Tris-HCl pH 8.0, 250 mM KCl, 10% glyercol, 7mM β-mercaptoethanol, and 350 mM imidazole. This eluent was loaded onto a 1 ml HiTrap heparin column and bound protein was eluted by a linear gradient of increasing KCl concentration to 770 mM. Fractions eluted from the heparin column judged by SDS-PAGE to be >90% pure full-length Pol λ were pooled and diluted as necessary to adjust the salt to 250 mM KCl before freezing. The Ku and XRCC4-ligase IV complexes were purified from baculovirus-infected cells as previously described [35].

Electrophoresis mobility shift assays (EMSA) were performed using a 60-bp double-stranded (ds) DNA substrate made by annealing 5' phosphorylated DAR166 (5'-CAGCTGGGAATTCCATATGAGTACTGCAGATGCACTTGCTCGATAGATCTAACATGAGCC-3') to DAR167 (5'Cy3-GTAGGGCTCATGTTAGATCTATCGAGCAAGTGCATCTGCAGTACTCATATGGAATTCCCAGCTGAG-3'). 10 nM of this substrate was incubated with 1 nM Ku for 5 minutes in a buffer containing 25 mM Tris-HCl pH 7.5, 150 mM KCl, 1% (wt/vol) polyethyleneglycol (molecular mass, greater than 8,000 kD; PEG), 1 mM DTT, 0.5 mg/mL bovine serum albumin (BSA), and 100nM EDTA, followed by addition of 500 ng uncut plasmid DNA, 10 nM XRCC4-ligase IV complex, and 50 nM of Pol λ followed by an additional incubation for 10 minutes on ice. Resulting DNA-protein complexes were separated by eletrophoresis on a 3.5% polyacrylamide gel in a buffer containing 30 mM Tris-borate (pH 8.2) and 0.3 mM EDTA (1/3X TBE), and detected using a Typhoon fluorescent imager (GE Biosciences).

The NHEJ assay employed a 300 bp substrate with the indicated end structures prepared as previously described [6], except substrates were fluorescently labeled by synthesis in a mix of 100 μM each dNTP supplemented with 50 μM Cy5 labeled dCTP (GE biosciences). End-joining assays were performed by incubating on ice 25 nM Ku and 5 nM DNA substrate in a buffer containing 25 mM Tris pH 7.5, 150 mM KCl, 1 mM DTT, 20 μg/ml BSA, 3% glycerol (v/v), 0.1 mM EDTA, 10% PEG (w/v) for 5 minutes, followed by addition of 50 nM X4-LIV, 25 nM Pol λ, and 500 ng of uncut plasmid DNA and a 10 minute incubation on ice. Reactions were then started by addition of 25 μM of each dNTP and 5mM $MgCl_2$ before incubation at 37 °C for 5 minutes. Samples were then de-proteinized and subject to electrophoresis on a non-denaturing 5% polyacrylamide gel. Substrate and product species were detected using a Typhoon fluorescent imager and quantified using ImageQuant Total Lab software (GE biosciences).

The following mutations of Pol λ were constructed and tested using EMSA and end-joining assays: L60A, L60F, Q64A, Q64L, R55A, and R57A. Potential structural changes due to the various mutations were assessed with 1D NMR using approximately 50 μM protein and a Varian 500 MHz spectrometer using the DPFGSE sequence for water suppression [36].

Crystallization trials with Pol λ BRCT domain

Unlabeled Pol λ BRCT protein was utilized in several high-throughput crystallization screens examining over 4000 conditions. No crystals were obtained.

Results

Chemical shift assignments and secondary structure

Figure 1 shows an annotated [^{1}H-^{15}N]-HSQC of the Pol λ BRCT domain. The chemical shift assignment procedure was generally facile and 90% complete, as assessed by CYANA. Most of the missing assignments correspond to the N-terminal three residues. In addition, Thr51, Gly52, and Arg55 in the loop preceding α-helix 1 (Figure 2, cyan) lack assignments, presumably due to conformational exchange broadening. Several shifts were noted to be unusual in that they are more than two standard deviations from the mean for that atom in the BioMagResBank (BMRB) database [37]. The shift of the Arg122 Hα is 1.93 ppm. The backbone of this residue is in a tight turn at the end of α-helix 3 and the ϕ/ψ angles are 57.9°/40.9°. These angles are within the acceptable range for Ramachandran plots, but are uncommon for an arginine residue; hence, the shift is outside the norm. The Hα shift of Ala46 (5.78 ppm) is unusual for an alanine residue, but not uncommon for other residue types within a β-sheet. This shift likely lies outside the mean for alanine because these residues are uncommon in β-sheets. Finally, the shift of 5.46 ppm for His82 Hδ2 is unusually low. His82, buried within the

protein core, is absolutely conserved and the Hδ2 proton probably experiences an upfield shift do to its proximity to the face of the indole ring of Trp114 (Figure 3). In addition, we were able to observe the typically labile Hδ1 proton of His82, which indicates a reduced exchange rate with water protons (Figure 1). NOE interactions were observed between the His82 Hδ1 and the methyl groups of Leu44, and the Hε2 and Hζ2 protons of Trp114, confirming the buried position of this proton. These interactions, combined with the slow exchange of Hδ1 support the presence of an H-bond connecting His82 Nδ1 and Arg45 C'.

Analysis of the overall fold of the Pol λ BRCT domain reveals an α/β/α motif (Figure 2), similar to the BRCT domains of Pol μ (PDB codes 2DUN and 2HTF [14]) and TdT (PDB code 2COE) (Figure 3A). The core of the domain is made up of a central β-sheet comprised of three short parallel β-strands, flanked by three α-helices. These secondary structural elements are arranged in a similar topography to the other Family X BRCT domains [14]. In addition to the core 3-stranded β-sheet, residues 71–73 (β-strand 2) and residues 95–97 (β-strand 5) have ϕ/ψ angles that are indicative of residues found in β-strands. However, given the positions of these strands relative to the core β-sheet, and the poor geometries for hydrogen bonding interactions, it is likely that these strands contribute little to the hydrogen bonding network of the β-sheet. Table 1 shows a summary of structural statistics for the ensemble of Pol λ BRCT domain structures. The experimental restraints show very few violations, and the covalent geometry is not strained. The ensemble RMSD for the 12 lowest energy structures refined by XPLOR-NIH is 0.68 Å over the backbone atoms of secondary structure elements.

A salt bridge that stabilizes the position of α-helix 1 in Pol μ (Glu36-Arg44) and TdT (Glu41-Arg49) is present but reversed in Pol λ (Arg50-Glu59). As noted above, Thr51, Gly52, and Arg55 in the loop preceding α-helix 1 in Pol λ were not structurally well-defined (Figure 2A, cyan) and are presumably subject to substantial exchange broadening. Interestingly, this region of the BRCT domain in Pol μ contains at least one residue (Arg43) that is important for efficient binding of NHEJ protein partners [14]. In the Pol μ BRCT domain structure, Arg43 is constrained by the salt bridge with Glu72. For Pol λ, the structurally corresponding residue is conserved (Arg57), however, this arginine is not similarly constrained. The position of the residue on loop L1, and the apparent flexibility of that loop lead to speculation as to whether Arg57 may mediate a similar interaction with the end-joining complex.

Structural stabilization by the C-terminus of the Pol λ BRCT

Initial studies of the Pol λ BRCT domain performed using shorter constructs that were designed based on consensus BRCT domains resulted in poor protein expression yields. We obtained an improved yield of soluble Pol λ BRCT using a longer construct that extended to Pro135. There are a number of hydrophobic interactions involving those C-terminal residues that would be expected to provide significant stability to the structure. These include interactions of Val125 and Val127 with Trp114, which are supported by NOEs between these residues. Phe130 also interacts with Ala113 and Leu117. Additional hydrophobic contacts link Ile132 to Val85 and/or Tyr91.

In addition, residues Ser131 and Ile132 have ϕ/ψ angles typical of β-strands, and in some structures of the calculated ensemble, make backbone hydrogen bonds indicative of a putative fifth β-strand, running antiparallel to β-strand 4, specifically Ile132:Leu109 and Lys111:Phe130. However, this two residue β-strand is not present in all simulations, so we conclude that this interaction, although intermittent, does provide some stabilization for the central ß-sheet. A similar anti-parallel β-strand composed of at least three residues (His112-Gln113-Leu114) also exists in the structure of TdT, but is less apparent in the structures of Pol μ, In the structure of Pol μ, however, there are several possible hydrogen bond interactions with the edge of the fourth β-strand. This type of ‘negative design’ is common among β-sheet proteins, and prevents the formation of insoluble aggregates in solution that may result from

edge-on interactions with other β-sheets [38]. Hydrogen exchange data also indicate that this region of the protein is dynamic, confirming the transient nature of β-strand 5 in Pol λ. In summary, the combination of a transient β-strand and multiple hydrophobic interactions provide important stabilization to the Pol λ BRCT domain. The poor expression noted for shorter constructs likely results from decreased stability of such truncated forms.

Conservation of sequence and structure across Family X BRCT domains

As noted above, there is 44% sequence identity between the polymerase and BRCT domains of Pol μ and TdT (Figure 3) [15]. Structures of the BRCT domains from TdT and Pol μ are very similar (Figure 3A); the lowest energy TdT structure superimposes on the average energy-minimized Pol μ structure with a backbone r.m.s.d. of 1.5 Å over 96 Cα atoms (see Footnote[1]). The main differences include a shorter α-helix 2 in the TdT domain, which also perturbs the position of the loop connecting α-helix 2 and β-strand 4 (L5). In the ensemble of Pol μ structures, this loop exhibits low sequence conservation (Figure 3B) and appears more disordered [14].

In contrast, the extent of sequence conservation is decreased when comparing Pol λ with either Pol μ or TdT. Sequence conservation is greater within the polymerase domains (Pol λ vs. Pol μ 30%; Pol λ vs. TdT 27%) than within the BRCT domains (Pol λ vs. Pol μ 23%; Pol λ vs. TdT 20%). When comparing residues across all three human Family X BRCT domains, there is very little conservation—a total of ten residues are fully conserved (12%, Figure 3B). .Of the ten conserved residues, five (His82, Val84, Leu109, Trp114, and Leu115) are buried within the core of the domain, and are likely important for correct folding and stability (Figure 3B). The other five (Gly54, Arg57, Gly69, Thr81, and V125) lie on the surface of the protein and are exposed to solvent. Studies of site-specific Pol μ mutants have demonstrated that Arg43, which aligns structurally with Arg57 in Pol λ, is important for binding to other components of the NHEJ complex and for subsequent end-joining by Pol μ in this complex [14]. Gly54 and Arg57 lie on the exposed loop preceding α-helix 1 (L1), and present a surface that presumably contributes to the binding interface. In general, there is little overall conservation of surface residues. The structure of Pol λ is less similar to that of TdT (r.m.s.d. of 2.0 Å over 72 Cα atoms) than to that of Pol μ (r.m.s.d. of 1.7 Å over 71 Cα atoms), which correlates with the degree of sequence similarity.

Structural differences among Family X BRCT domains

Though the overall folds of the three Family X BRCT domains are highly conserved (Figure 3A), there are small differences in the positioning of secondary structural elements. The most notable difference occurs in the positioning of α-helix 2 of the Pol λ BRCT domain, which runs almost perpendicular to the direction of the core β-strands. In Pol μ and TdT, α-helix 2 is nearly antiparallel to the direction of the core β-strands. In order to confirm the positioning and direction of α-helix 2, the residual dipolar couplings of residues in secondary structural elements were fit to the CYANA structures that were calculated without utilizing the RDCs. The agreement was very good, generally showing a strong positive correlation ($r > 0.6$) for calculated versus measured RDCs. Errors for residues in α-helix 2 were not greater than for other couplings, indicating the validity of the displayed orientation. The model was subsequently refined with XPLOR-NIH using the RDCs. Comparison of the structures before and after refinement shows that the protein fold was only subtly altered, although the agreement of the calculated and measured RDCs improves to greater than 0.99. The region of the Pol λ BRCT domain containing α-helix 2 exhibits the least sequence conservation across the Family

[1]All superpositions of the Family X BRCT domains were preformed using the superposition algorithm in O [39] T. Jones, J. Zou, S. Cowan and M. Kjeldgaard Acta Crystallogr. Sect. A. 47 (1991) 110–119., and were base on β-strands 1 and 3 of the lowest energy structure from the ensemble.

X BRCT domains (Figure 3). Therefore, it is not surprising that this particular region of the BRCT domains would show a lower degree of structural conservation. Given that the sequence conservation of α-helix 2 is so low across the BRCT domain superfamily as to be nearly undetectable [9], it seems unlikely that this region of the polymerase could dock with similar structures. α-Helix 2 probably plays a structurally protective role, covering the hydrophobic core β-sheet.

As would be expected from regions of low sequence conservation, structural disparities are also apparent in loop regions of the Family X BRCT domains. For example, the loop between β-strand 1 and α-helix 1 (L1) differs significantly among the Family X BRCT domains, primarily due to the lack of homology within the N-terminal end of α-helix 1 (Figure 4A). In Pol λ, α-helix 1 is positioned at a slightly different angle than the corresponding helix in Pol μ and TdT. Interestingly, there is a slight deviation from ideal α-helical geometry near the N-terminal end of this helix. This deviation occurs at Leu60-Phe61, and is not present in Pol μ or TdT.

The most significant structural differences among the Family X BRCT domains are located between α-helix 2 and β-strand 4 (Figure 4B). The length, residue composition, and conformation of this loop vary widely among Pol μ, TdT, and Pol λ. Ostensibly, some variation of this loop region is due to the differences in the termination of α-helix 2. Though the orientation of this helix is similar in Pol μ and TdT, α-helix 2 in Pol λ is shorter and lies nearly perpendicular to the plane of the direction of the β-strands, creating a loop region with a vastly different conformation. Interestingly, in Pol μ and Pol λ, this loop contains a PPG (Pol μ: Pro91-Gly93, Pol λ: Pro104-Gly106) motif that is absent in TdT (Figure 3B). This PPG motif generates a similar structure in Pol μ and Pol λ, but the position of the motif is laterally displaced. For Pol μ and Pol λ, the loop bridging α-helix 2 and β-strand 4 is proline-rich; not so in this region of TdT. The high concentration of proline residues in this region is intriguing, given that proline-rich sequences have been found to serve as recognition motifs for protein binding partners [40].

Role of α-helix 1 in interactions with NHEJ binding partners

Structural characterization of the Pol μ BRCT domain revealed two solvent-exposed hydrophobic residues on α-helix 1, Phe46 and Leu50 which, along with conserved Arg43, were postulated to be important components of the interaction surface of this domain. Further support for this conclusion was derived from the observation that the BRCT domain of TdT has similarly positioned hydrophobic residues on α-helix 1 (see Footnote[2]). These key residues in Pol μ were mutated to alanine and found to be important both for binding with the XRCC4-Ligase IV components of the NHEJ complex, and for functional activation [14]. Because these amino acids are structurally conserved in the BRCT domain of TdT, we hypothesize that these polymerases would interact with the NHEJ repair complex in similar fashions.

The situation is somewhat less clear for Pol λ, for which only two of these positions have a homologous residue: Arg57 and Leu60 (Arg43 and Phe46 conserved in Pol μ) (Figure 3B and 5A). For Pol λ, the corresponding R57A mutant showed dramatically impaired complex formation (Figure 5B). Meanwhile, the effect of the L60A substitution was slightly less detrimental. Interestingly, the L60F mutant, designed to mimic Phe46 of Pol μ, exhibited complex formation more similar to that of wildtype. This pattern differs from that seen with Pol μ, for which the F46A mutation is significantly more perturbing than the R43A mutation [14]. Other similarities to Pol μ that were probed for their importance in NHEJ complex

[2]According to published sequence alignments (e.g. Figure 3B), these residues are both conserved in TdT. However, the structure deposited in the Protein Data Bank (PDB code 2COE) has leucine residues at both positions.

formation were Gln64 in Pol λ, structurally homologous to Leu50 in Pol μ; and Arg55 in Pol λ, which forms a salt bridge with Asp86 similar to the Arg43-Glu72 interaction in Pol μ (see figure 5A). Alanine substitution mutation of Arg55 and Gln64 in Pol λ showed no disruption of complex formation, suggesting they are unlikely to contribute significantly to the interaction. Mutation of Q64L, which would correspond to Leu50 in Pol μ, neither enhanced nor perturbed complex formation.

Logically, nonhomologous end-joining activity should correlate with efficient NHEJ complex formation. Therefore, the Pol λ BRCT domain mutants were tested for their end-joining activity. Alanine mutants of either Arg57 or Leu60 of Pol λ showed greatly diminished end-joining activity, relative to the enzyme with the wild-type BRCT domain. Indeed, the R57A mutation displayed the weakest end-joining activity (Figure 5C). The L60A mutant was slightly more active. As might be expected from similar experiments using Pol μ, the L60F substitution mutant was more efficient in both complex formation and end-joining activity than L60A [14]. Similar to the results in NHEJ complex formation, R55A and Q64A/L displayed similar end-joining activity to that of wildtype Pol λ. In summary, the performance of the mutants BRCT domains in the activity assay parallels the complex formation in the binding assay.

In order to assess whether any of these mutations produced significant structural perturbations, we acquired ^{1}H NMR spectra of each protein for comparison. In the 1D spectrum, Leu115 is easily identifiable (See Supplementary Figure 1) because it is strongly shifted upfield due to interaction with Phe61 on α-helix 1, where the mutations were made. This shift should be particularly sensitive to potential structural changes in α-helix 1. None of the mutants show significant changes in the overall ^{1}H spectra, or in the shift of Leu115, CD1 (Supp. Figure 1), supporting the conclusion that these mutations did not introduce major structural changes in the domain.

Determination of the oligomerization state by ^{15}N relaxation analysis

The structural analysis presented here is based on the assumption that the BRCT domain is monomeric. This assumption is consistent with relaxation data (R_1 and R_2) measured at 11.7 T, which yielded an isotropic rotational correlation time of 10.0 ns [41,42]. This result is also consistent with our previous analysis of relaxation data for the Pol μ BRCT domain, performed at an identical temperature (10°C), which yielded a rotational correlation time of 10.5 ns [14]. In addition, static and dynamic light scattering data for the Pol μ BRCT domain confirmed its monomeric oligomerization state.

Analysis of structural dynamics

Based on the isotropic diffusion of the Pol λ BRCT domain, the relaxation data may be further interpreted to analyze internal dynamics. Two regions of the protein exhibited decreased NOE ratios, indicative of more rapid internal motion: the N-terminus and residues Gln76 and Gly77 (Suppl. Figure 2). Complete “model-free” analysis of ^{15}N R_1, R_2 and NOE data [43] produced no new insights beyond the increased dynamics of the aforementioned residues (data not shown). Gln76 and Gly77 are located on the loop between β-strands 2 and 3. In the ensemble of structures, these residues are poorly defined (Figure 2A, green).

CPMG experiments, designed to measure rates of conformational exchange on the millisecond to microsecond time scale, showed more variation than the ps – ns motions derived from the “model-free” analysis. Fourteen amide sites exhibit typical dispersion curves (Suppl. Figure 3A). These curves indicate conformational exchange, but as reviewed by Kempf, et al [44], it is difficult to fit exact rates when the shapes are similar to exponential decay. The rest of the measurable amide sites yielded dispersion curves closer to flat lines (Suppl. Figure 3B), indicating no detectable conformational change.

On the face of the protein that exhibits less sequence conservation (i.e. the regions containing α-helix 2), the residues with dispersion curves clustered near the intersection of the two proline-rich loops, P_{74}AQGPG and P_{101}QLPPGA (Figure 4A, Figure 6A, and Suppl. Figure 3). Interestingly, residues Arg45, Thr81, and Gly106 adjacent to these loops show multiple peaks in the ^{1}H-^{15}N HSQC spectra, indicative of slow exchange (Figure 1). In these cases, the ^{13}C shifts of the residues in the HNCACB experiment were similar enough that the extra peaks could be confidently assigned to each residue (Figure 6A, colored yellow). The backbone atoms of these three residues are in close proximity and are one or two residues displaced from the residue beginning each β-strand. It is likely that these slow exchange conformers are related to proline isomerization.

In contrast, on the opposite face of the β-sheet, there is a higher level of sequence conservation, and decreased conformational exchange broadening. One exception to this involves a patch of mostly hydrophobic surface-exposed residues including Leu117, Phe130, and Glu87 (Figure 6B, colored pink) that show conformational exchange in CPMG experiments (Suppl. Figure 3). In addition, Gly129 (Figure 6B, colored yellow) exhibits an extremely broad peak in comparison to other glycine residues (Figure 1). The amide resonance of Ala113, which lies in a congested region of the spectrum, is split into two slowly exchanging components. Since there are no proline residues in the vicinity of Ala113, this heterogeneity is unlikely to correspond to proline isomerism, but may relate to alternate conformations of some of the nearby aromatic residues such as Trp114 or Phe140. Overlap of the Ala113 resonance with other amide peaks (Figure 1, inset) limited the relaxation studies of this residue.

Discussion

With the solution structure of the Pol λ BRCT domain, we now have a complete portrait of the human Family X BRCT domains. In general, the structural and electrostatic characteristics of the exposed surface support the conclusion that they can serve as alternate polymerases by docking with a common binding site in the NHEJ complex. Further, structural and mutation data for the Pol μ and Pol λ BRCT domains demonstrate the importance of residues along and near α-helix 1 in mediating the roles of these polymerases in NHEJ. Nevertheless, the fact that each of the BRCT domains contains unique structural features indicates that they do not serve as equivalent, interchangeable modules. Furthermore, based on the degree of sequence and structural homology determined in the present study, the BRCT domain of Pol λ is more dissimilar than the other two members of the Pol X family.

The work presented here further substantiates the proposed protein-protein interaction surface linking the Family X BRCT domains to the NHEJ complex of Ku/XRCC4/Ligase IV [14]. According to the proposed hypothesis, the ‘shoulder’ of the Pol μ BRCT domain involved in binding the NHEJ complex is formed by the C-terminal end of β-strand 1, the N-terminal half of α-helix 1, and the loop connecting these two structural elements. The BRCT domains of Pol μ/TdT each contain three conserved, surface-exposed residues: Arg43/Arg48, Phe46/Phe51 and Leu50/Leu55 that, when mutated to alanine, disrupt formation of the NHEJ complex at the sites of DSBs [14]. The BRCT domain of Pol λ, contains an arginine residue (Arg57) similarly positioned at the N-terminal end of α-helix 1, but with Leu60 substituting for Phe46 in Pol μ. The conservative substitution of Leu for Phe is likely to be sufficient to support binding to the same receptor and, as demonstrated above, L60A reduces binding, although the effect is considerably less dramatic than the effect of the F46A mutation in Pol μ. In contrast, the third conserved leucine residue is nonconservatively replaced by Gln64 in Pol λ, which when mutated to alanine, was shown to be unimportant for binding the NHEJ complex. Therefore, comparing the effects of corresponding mutations at the homologous positions of Pol μ and Pol λ on XRCC4-Ligase IV binding suggests a model characterized by a significant affinity gradient along α-helix 1, so that the interaction near the N-terminus is relatively enhanced,

becoming progressively weaker moving down the helix (Figure 7). One possible interpretation is that the specific interaction surface created by the key residues in Pol λ may yield a greater shape complementarity with the NHEJ complex. Another possible theory is that α-helix 1 may tilt away from the interaction surface, perhaps as a consequence of stronger and/or additional interactions with the preceding flexible loop. Structural elements exhibiting enhanced flexibility such as the BRCT Loop 1 are thought to facilitate induced-fit recognition, and this type of behavior has been noted in a variety of other systems, e. g. chemokines [45] and fibronectins [46].

In general, it is not surprising that the BRCT domains of each polymerase should bind to the same site, since the enzymes ultimately perform a similar polymerization function. However, some differences should exist that select for a particular polymerase depending on the details of the substrate structure. An alternative binding mode may have developed as a method to make the more accurate Pol λ the preferred polymerase under certain conditions. A second factor to be considered is the differing substrate specificities exhibited by Pol μ and Pol λ. Of these two polymerases, Pol μ has the ability to bind and resolve DSBs where no complementarity exists between the two ends [6,47]. However, Pol λ requires at least a single complementary base pair at the site of the DSB [6]. A variation in the BRCT domain interaction with other components of the NHEJ complex might cause alterations that could allow greater access for the polymerase domain at the site of the DSB, dependent on the structure of the DSB requiring repair. Additionally, the extended length of the Pro/Ser-rich linker connecting the Pol λ BRCT and polymerase domains could influence such alterations. A final factor to consider is the putative role of Pol λ in BER, which would presumably involve a different set of interactions and a different docking site. This explanation is consistent with the more significant structural differences noted above between the BRCT domain of Pol λ compared with that of Pol μ and TdT.

With this contribution, there is structural information available for all of the Family X polymerization domains, and for each of the three BRCT domains. In addition, the completion of the Family X structural portrait, including the polymerase domains, was achieved through the cooperative contributions of X-ray crystallography [15] and NMR spectroscopy [14]. By means of this approach, we have discovered a means to elucidate the catalytic mechanism; the intricacies of nucleotide incorporation fidelity; the structural contributions to selection of DNA substrates; and the basis of interactions with other proteins which endow biological function. Studies directed at determining the structure of the multi-component NHEJ complex are currently in progress.

Supplementary Material

Refer to Web version on PubMed Central for supplementary material.

Acknowledgments

We thank Thomas Kirby, Robert Petrovich, Lori Edwards, and the Protein Expression Core Facility for their efforts in optimizing protein expression. We also thank William Beard and Katarzyna Bebenek for critical reading and thoughtful comments on the manuscript. This research was supported in part by NIH grant # CA97096 (to D.A.R) and by the Intramural Research Program of the NIH, National Institute of Environmental Health Sciences. Dr. DeRose's contribution was funded in whole with the Federal funds from NIH/NIEHS, under Delivery Order HHS27300700046U to Constella Group, LLC.

Works Cited

1. Braithwaite EK, Prasad R, Shock DD, Hou EW, Beard WA, Wilson SH. DNA polymerase lambda mediates a back-up base excision repair activity in extracts of mouse embryonic fibroblasts. J Biol Chem 2005;280:18469–18475. [PubMed: 15749700]

2. Srivastava DK, Berg BJ, Prasad R, Molina JT, Beard WA, Tomkinson AE, Wilson SH. Mammalian abasic site base excision repair. Identification of the reaction sequence and rate-determining steps. J Biol Chem 1998;273:21203–21209. [PubMed: 9694877]

3. Mahajan KN, Nick McElhinny SA, Mitchell BS, Ramsden DA. Association of DNA polymerase mu (pol mu) with Ku and ligase IV: role for pol mu in end-joining double-strand break repair. Mol Cell Biol 2002;22:5194–5202. [PubMed: 12077346]

4. Fan W, Wu X. DNA polymerase lambda can elongate on DNA substrates mimicking non-homologous end joining and interact with XRCC4-ligase IV complex. Biochem Biophys Res Commun 2004;323:1328–1333. [PubMed: 15451442]

5. Lee JW, Blanco L, Zhou T, Garcia-Diaz M, Bebenek K, Kunkel TA, Wang Z, Povirk LF. Implication of DNA polymerase lambda in alignment-based gap filling for nonhomologous DNA end joining in human nuclear extracts. J Biol Chem 2004;279:805–811. [PubMed: 14561766]

6. Nick McElhinny SA, Havener JM, Garcia-Diaz M, Juarez R, Bebenek K, Kee BL, Blanco L, Kunkel TA, Ramsden DA. A gradient of template dependence defines distinct biological roles for family X polymerases in nonhomologous end joining. Mol Cell 2005;19:357–366. [PubMed: 16061182]

7. Bertocci B, De Smet A, Weill JC, Reynaud CA. Nonoverlapping functions of DNA polymerases mu, lambda, and terminal deoxynucleotidyltransferase during immunoglobulin V(D)J recombination in vivo. Immunity 2006;25:31–41. [PubMed: 16860755]

8. Schatz DG. V(D)J recombination. Immunol Rev 2004;200:5–11. [PubMed: 15242391]

9. Bork P, Hofmann K, Bucher P, Neuwald AF, Altschul SF, Koonin EV. A superfamily of conserved domains in DNA damage-responsive cell cycle checkpoint proteins. Faseb J 1997;11:68–76. [PubMed: 9034168]

10. Rooney S, Chaudhuri J, Alt FW. The role of the non-homologous end-joining pathway in lymphocyte development. Immunol Rev 2004;200:115–131. [PubMed: 15242400]

11. Ma Y, Lu H, Schwarz K, Lieber MR. Repair of double-strand DNA breaks by the human nonhomologous DNA end joining pathway: the iterative processing model. Cell Cycle 2005;4:1193–1200. [PubMed: 16082219]

12. Nick McElhinny SA, Ramsden DA. Sibling rivalry: competition between Pol X family members in V(D)J recombination and general double strand break repair. Immunol Rev 2004;200:156–164. [PubMed: 15242403]

13. Ma Y, Lu H, Tippin B, Goodman MF, Shimazaki N, Koiwai O, Hsieh C, Schwarz K, Lieber MR. A biochemically defined system for mammalian nonhomologous DNA end-joining. Mol Cell 2004;16:701–713. [PubMed: 15574326]

14. Derose EF, Clarkson MW, Gilmore SA, Galban CJ, Tripathy A, Havener JM, Mueller GA, Ramsden DA, London RE, Lee AL. Solution Structure of Polymerase mu's BRCT Domain Reveals an Element Essential for Its Role in Nonhomologous End Joining. Biochemistry 2007;46:12100–12110. [PubMed: 17915942]

15. Moon AF, Garcia-Diaz M, Batra VK, Beard WA, Bebenek K, Kunkel TA, Wilson SH, Pedersen LC. The X family portrait: Structural insights into biological functions of X family polymerases. DNA Repair (Amst). 2007

16. Pascal SM, Muhandiram R, Yamazaki T, Forman-Kay JD, Kay LE. Simultaneous acquisition of 15N- and 13C-edited NOE spectra of proteins dissolved in H2O. J. Magn. Reson. Ser. B 1994;103:197–201.

17. Farrow NA, Muhandiram R, Singer AU, Pascal SM, Kay CM, Gish G, Shoelson SE, Pawson T, Forman-Kay JD, Kay LE. Backbone dynamics of a free and phosphopeptide-complexed Src homology 2 domain studied by 15N NMR relaxation. Biochemistry 1994;33:5984–6003. [PubMed: 7514039]

18. Loria JP, Rance N, Palmer AG III. Relaxation-compensated Carr-Purcell Meiboom-Gill sequence for characterizing chemical exchange by NMR spectroscopy. J. Am. Chem. Soc 1999;121:2331–2332.

19. Mulder FA, Skrynnikov NR, Hon B, Dahlquist FW, Kay LE. Measurement of slow (micros-ms) time scale dynamics in protein side chains by (15)N relaxation dispersion NMR spectroscopy: application to Asn and Gln residues in a cavity mutant of T4 lysozyme. J Am Chem Soc 2001;123:967–975. [PubMed: 11456632]

20. Permi P. A spin-state-selective experiment for measuring heteronuclear one-bond and homonuclear two-bond couplings from an HSQC-type spectrum. J. Biomol. NMR 2002;22:27–35. [PubMed: 11885978]
21. Hansen MR, Mueller L, Pardi A. Tunable alignment of macromolecules by filamentous phage yields dipolar coupling interactions. Nat Struct Biol 1998;5:1065–1074. [PubMed: 9846877]
22. Wittekind M, Mueller L. HNCACB, a high-sensitivity 3D NMR experiment to correlate amide-proton and nitrogen resonances with the alpha-carbon and beta-carbon resonances in proteins. J. Magn. Reson. Ser. B 1993;101:201–205.
23. Grzesiek S, Bax A. Correlating backbone amide and side chain resonances in larger proteins by multiple relayed triple resonance NMR. J. Am. Chem. Soc 1992;114:6291–6293.
24. Johnson BA, Blevins RA. NMRVIEW: a computer program for the visualization and analysis of NMR data. J. Biomol. NMR 1994;4:603–614.
25. Vuister GW, Bax A. Quantitative J correlation: a new approach for measuring homonuclear three-bond J(HNHalpha) coupling constants in 15N-enriched proteins. J Am Chem Soc 1993;115:7772–7777.
26. Grzesiek S, Anglister J, Bax A. Correlation of backbone amide and aliphatic side-chain resonances in 13C/15N-enriched proteins by isotropic mixing of 13C magnetization. J. Magn. Reson. Ser. B 1993;101:114–119.
27. Logan TM, Olejniczak ET, Xu RX, Fesik SW. A general method for assigning NMR spectra of denatured proteins using 3D HC(CO)NH-TOCSY triple resonance experiments. J Biomol NMR 1993;3:225–231. [PubMed: 8477187]
28. Logan TM, Olejniczak ET, Xu RX, Fesik SW. Side chain and backbone assignments in isotopically labeled proteins from two heteronuclear triple resonance experiments. FEBS Lett 1992;314:413–418. [PubMed: 1281793]
29. Montelione GT, Lyons BA, Emerson SD, Tashiro M. An efficient triple resonance experiment using 13C isotropic mixing for determining sequence-specific resonance assignments of isotopically enriched proteins. J. Am. Chem. Soc 1992;114:10974–10975.
30. Yamazaki T, Forman-Kay JD, Kay LE. Two-dimensional NMR experiments for correlating 13Cbeta and 1Hdelta/epsilon chemical shifts of aromatic residues in 13C-labeled proteins via scalar couplings. J. Am. Chem. Soc 1993;115:11054–11055.
31. Zwahlen C, Gardner KH, Sarma SP, Horita DA, Byrd RA, Kay LE. An NMR experiment for measuring methyl-methyl NOEs in 13C labeled proteins with high resolution. J. Am. Chem. Soc 1998;120:7617–7625.
32. Herrmann T, Guntert P, Wuthrich K. Protein NMR structure determination with automated NOE assignment using the new software CANDID and the torsion angle dynamics algorithm DYANA. J Mol Biol 2002;319:209–227. [PubMed: 12051947]
33. Schwieters CD, Kuszewski JJ, Tjandra N, Clore GM. The Xplor-NIH NMR molecular structure determination package. J Magn Reson 2003;160:65–73. [PubMed: 12565051]
34. Cornilescu G, Delaglio F, Bax A. Protein backbone angle restraints from searching a database for chemical shift and sequence homology. J Biomol NMR 1999;13:289–302. [PubMed: 10212987]
35. Nick McElhinny SA, Snowden CM, McCarville J, Ramsden DA. Ku recruits the XRCC4-ligase IV complex to DNA ends. Mol Cell Biol 2000;20:2996–3003. [PubMed: 10757784]
36. Dalvit C. Efficient multiple-solvent suppression for the study of the interactions of organic solvents with biomolecules. Journal of Biomolecular Nmr 1998;11:437–444.
37. Seavey BR, Farr EA, Westler WM, Markley JL. A relational database for sequence-specific protein NMR data. J. Biomol. NMR 1991;1:217–236. [PubMed: 1841696]
38. Richardson JS, Richardson DC. Natural beta-sheet proteins use negative design to avoid edge-to-edge aggregation. Proc. Nat. Acad. Sci 2002;99:2754–2759. [PubMed: 11880627]
39. Jones T, Zou J, Cowan S, Kjeldgaard M. Acta Crystallogr. Sect. A 1991;47:110–119. [PubMed: 2025413]
40. Kay BK, Williamson MP, Sudol M. The importance of being proline: the interaction of proline-rich motifs in signaling proteins with their cognate domains. Faseb J 2000;14:231–241. [PubMed: 10657980]

41. Tjandra N, Feller SE, Pastor RW, Bax A. Rotational diffusion anisotropy of human ubiquitin from N-15 NMR relaxation. J Am Chem Soc 1995;117:12562–12566.

42. Kroenke CD, Loria JP, Lee LK, Rance N, Palmer AG III. Longitudinal and transverse 1H-15N dipolar/15N chemical shift anisotropy relaxation interference: Unambiguous determination of rotational diffusion tensors and chemical exchange effects in biological macromolecules. J Am Chem Soc 1998;120:7905–7915.

43. Lipari G, Szabo A. Model-free approach to the interpretation of nuclear magnetic resonance relaxation in macromolecules. 1. Theory and range of validity. J Am Chem Soc 1981;104:4546–4559.

44. Kempf JG, Loria JP. Protein dynamics from solution NMR: theory and applications. Cell Biochem Biophys 2003;37:187–211. [PubMed: 12625627]

45. Clark-Lewis I, Kim KS, Rajarathnam K, Gong JH, Dewald B, Moser B, Baggiolini M, Sykes BD. Structure-activity relationships of chemokines. J Leukoc Biol 1995;57:703–711. [PubMed: 7759949]

46. Carr PA, Erickson HP, Palmer AG 3rd. Backbone dynamics of homologous fibronectin type III cell adhesion domains from fibronectin and tenascin. Structure 1997;5:949–959. [PubMed: 9261088]

47. Moon AF, Garcia-Diaz M, Bebenek K, Davis BJ, Zhong X, Ramsden DA, Kunkel TA, Pedersen LC. Structural insight into the substrate specificity of DNA polymerase mu. Nat Struct Mol Biol 2007;14:45–53. [PubMed: 17159995]

48. Laskowski RA, MacArthur MW, Moss DS, Thornton JM. PROCHECK: a program to check the stereochemical quality of protein structures. J. Appl. Cryst 1993;26:283–291.

49. DeLano, WL. DeLano Scientif. San Carlos, CA, USA: 2002. The PyMOL Molecular Graphic System User's Manual.

50. Kraulis P. MOLSCRIPT: a program to produce both detailed and schematic plots of proteins. J Appl Crystallogr 1991;24:946–950.

51. Merritt EA, Murphy ME. Raster3D Version 2.0. A program for photorealistic molecular graphics. Acta Crystallogr D Biol Crystallogr 1994;50:869–873. [PubMed: 15299354]

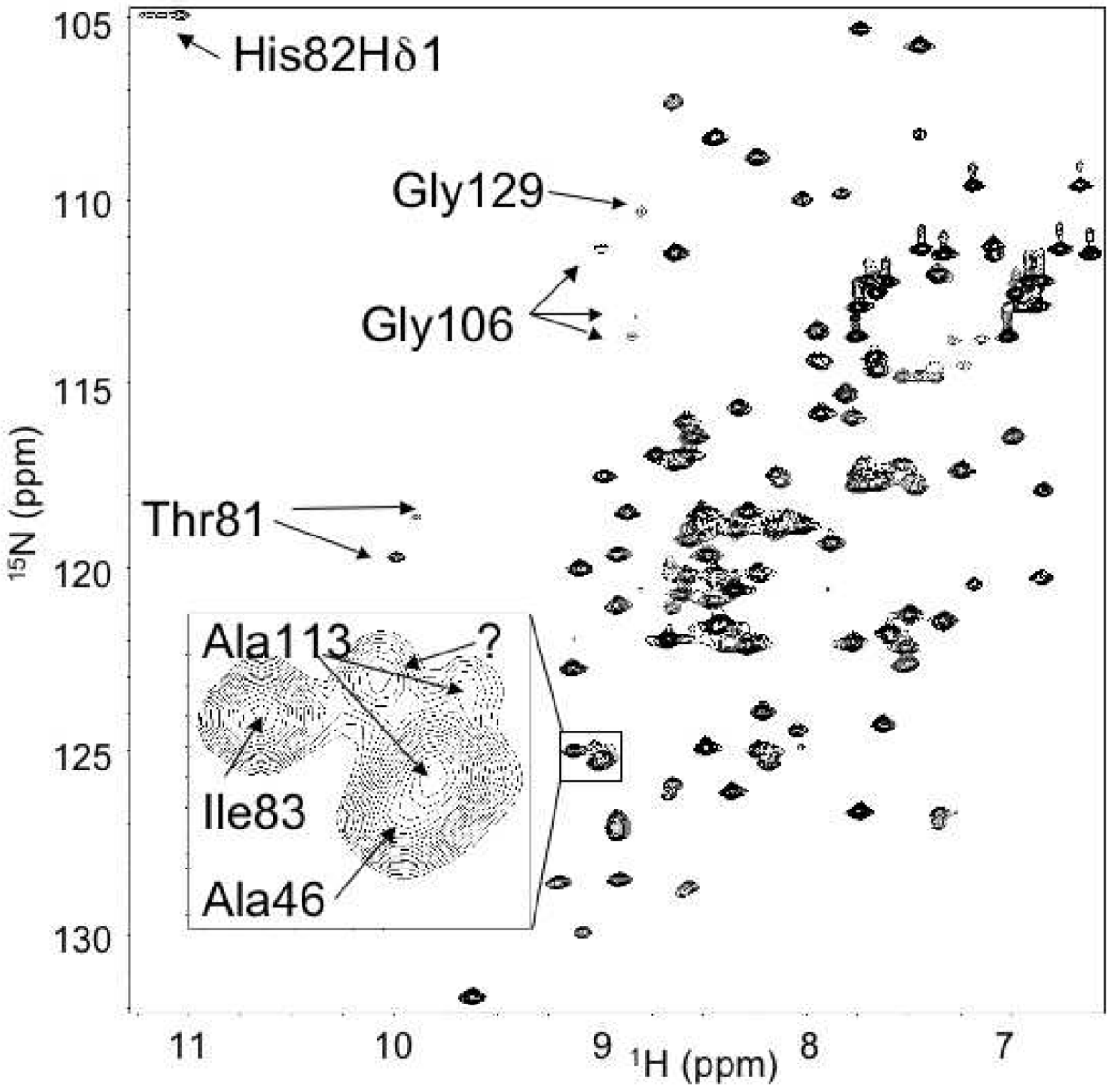

Figure 1.
Annotated HSQC of [^{1}H-^{15}N]-Pol λ BRCT domain. Inset: Expanded view of degenerate peaks surrounding Ala113.

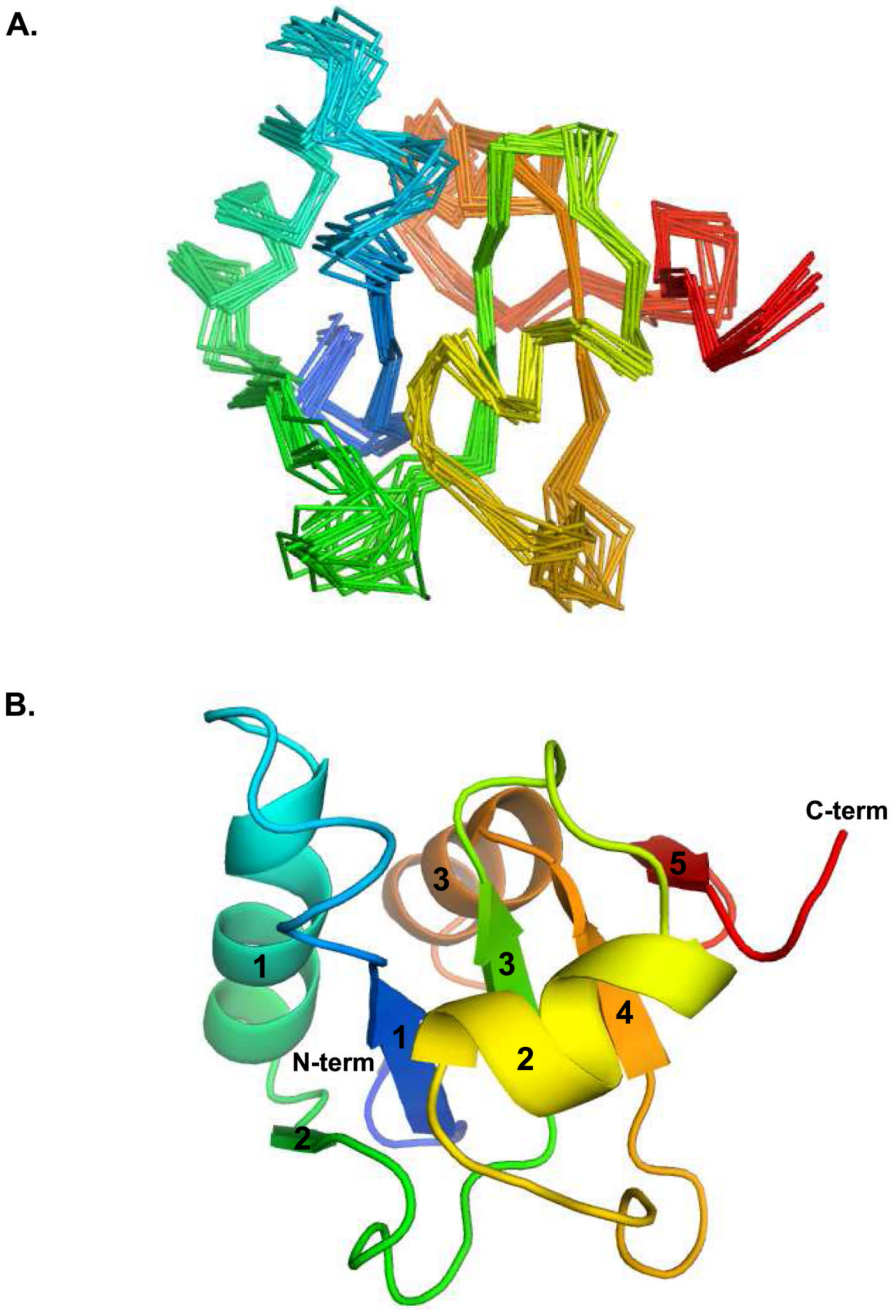

Figure 2.
Ensemble and secondary structure of Pol λ BRCT domain. (A) The ensemble of structures shows good convergence with the exception of a few loops. (B) The core parallel β-sheet characteristic of BRCT domains is well determined. The lowest energy structure from the ensemble was used to generate this image, using PyMOL [49]. The secondary structural elements are shaded from blue to red; α-helices and β-strands are labeled numerically.

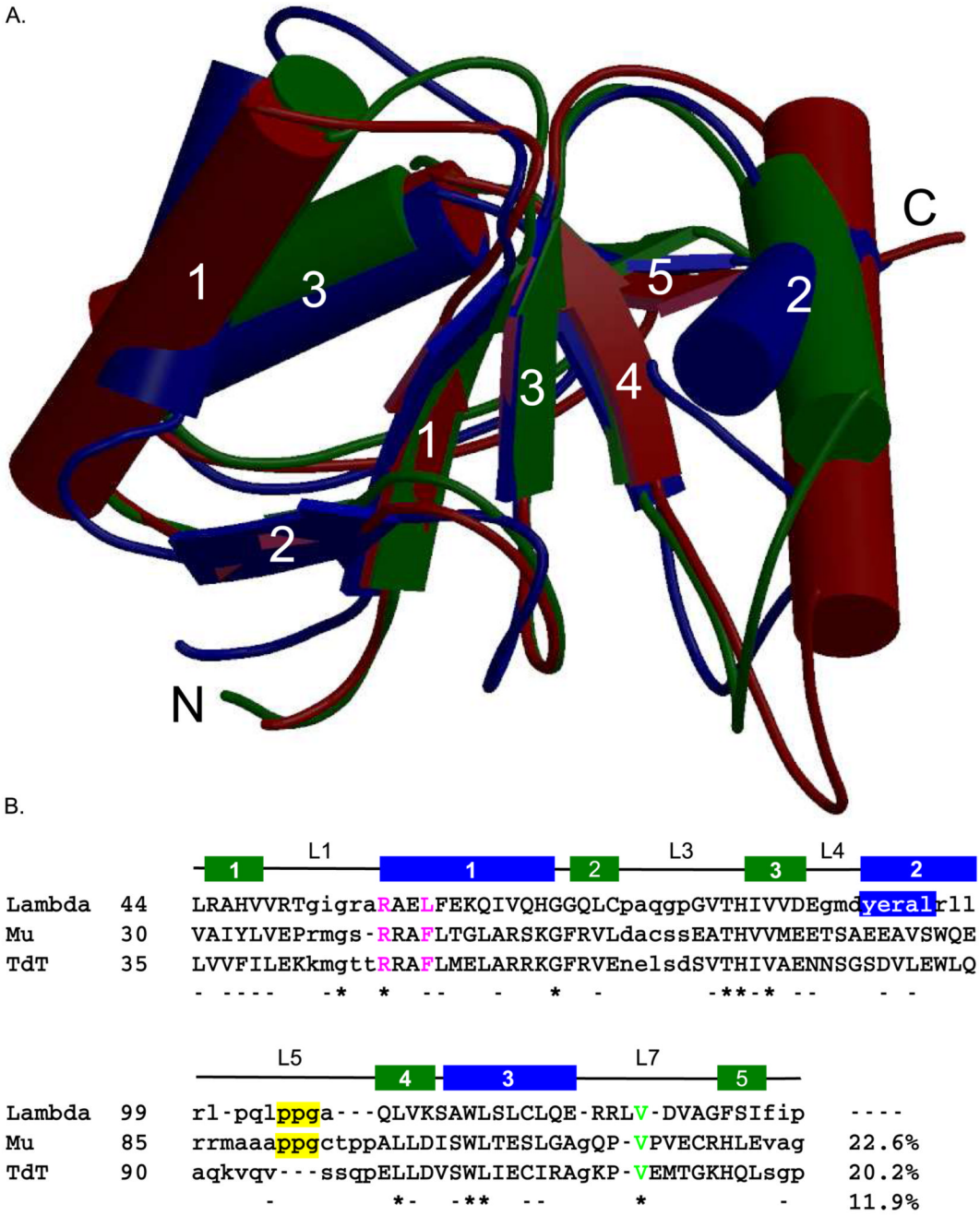

Figure 3.

Structural alignment of the BRCT domains of the Family X polymerases. (A). Superposition of the BRCT domains from human Pol μ (PDB code 2DUN, maroon), TdT (PDB code 2COE, green), and Pol λ (PDB code 2JW5, blue). α-helices (cylinders) and β-strands (directional arrows) are labeled numerically. This figure was created using MolScript [50] and Raster3D [51] (B). Structure-based primary sequence alignment. The positions of the conserved secondary structural elements of the Pol λ BRCT domain are shown as follows: β-strands are drawn as green boxes and α-helices are drawn as blue boxes. Structurally homologous residues are in capital letters, while nonhomologous regions are shown in lower-case letters. Absolutely conserved residues are indicated by asterisks below the alignment, and nearly conserved

residues are dashed. The PPG motif is boxed in yellow. The conserved valine residue required for protein stability is shown in green. Residues mutated for biochemical analysis of binding to NHEJ protein partners are in magenta.

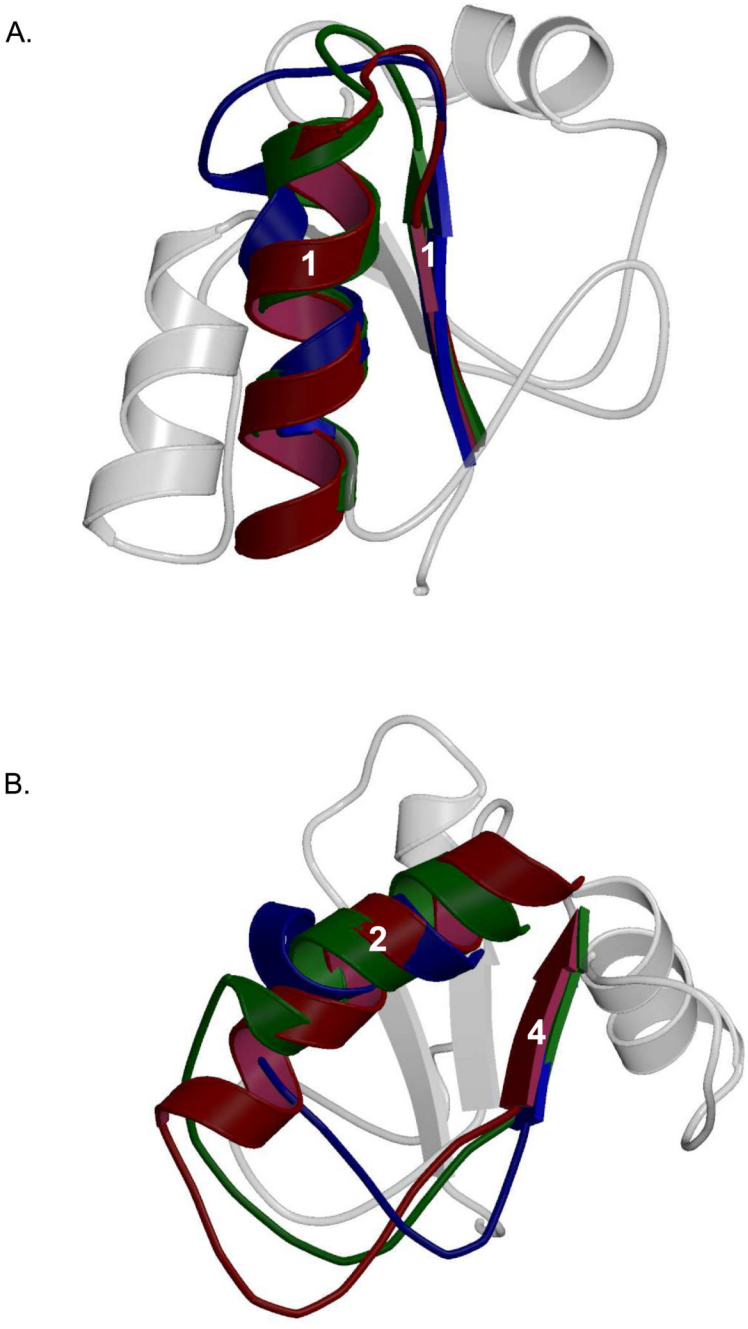

Figure 4.
Comparison of the structural differences seen in Family X BRCT domain loop regions. Secondary structural elements of Pol λ BRCT are shown in the background in light gray. (A). Superposition of the loop between β-strand 1 and α-helix 1 in Pol μ (PDB code 2DUN, maroon), TdT (PDB code 2COE, green), and Pol λ (PDB code 2JW5, blue). (B). Superposition of the loop between α-helix 2 and β-strand 4 in Pol μ (PDB code 2DUN, maroon), TdT (PDB code 2COE, green), and Pol λ (PDB code 2JW5, blue).

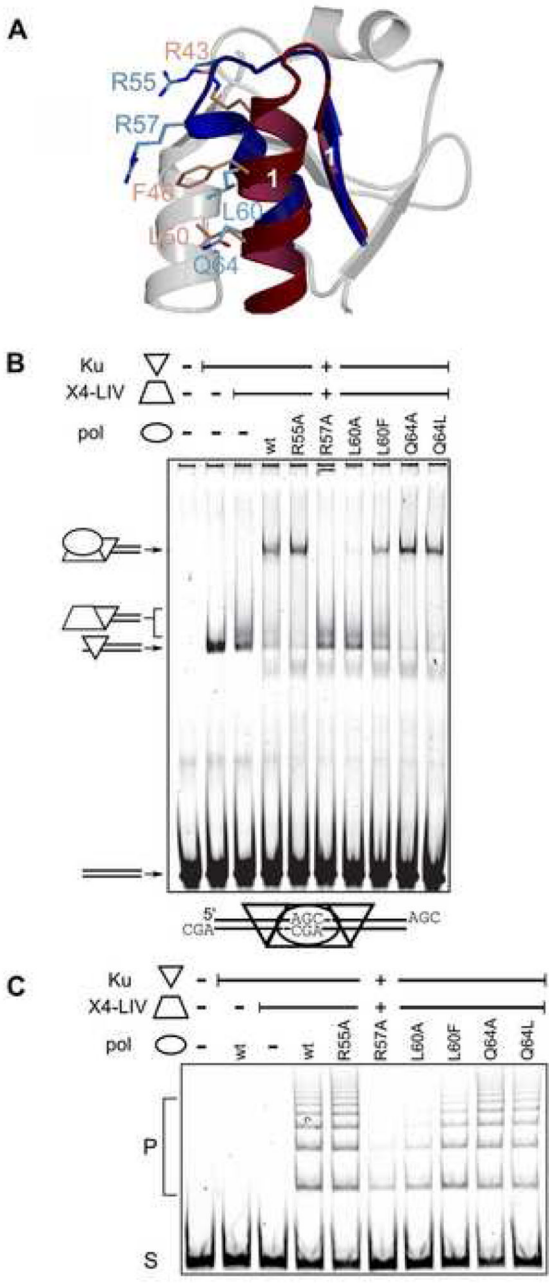

Figure 5.

NHEJ activity of Pol λ BRCT domain mutants. (A). Pol λ (PDB code 2JW5), blue) superimposed with Pol μ (PDB code 2DUN, maroon). Residues in α-helix 1 crucial for interaction with core NHEJ factors in Pol μ (R43, F46, and L50, light red) are shown with sticks, relative to tested positions in Pol λ (R55, R57, L60 and Q64, light blue). Secondary structural elements of Pol λ BRCT are shown in the background in light gray. (B). EMSA analysis was performed in the presence of a 60 bp DNA duplex, Ku and the XRCC4-ligase IV (X4-LIV) complex and various full-length Pol λ proteins. . The composition of each species of distinct mobility is noted with cartoons at the left of the panel. C) Joining of a 300 bp substrate with three nucleotide AGC 3' overhangs was performed in the presence of Ku, XRCC4-Ligase

IV, and various full-length Pol λ constructs as noted. S, substrate, P, joined concatemer products.

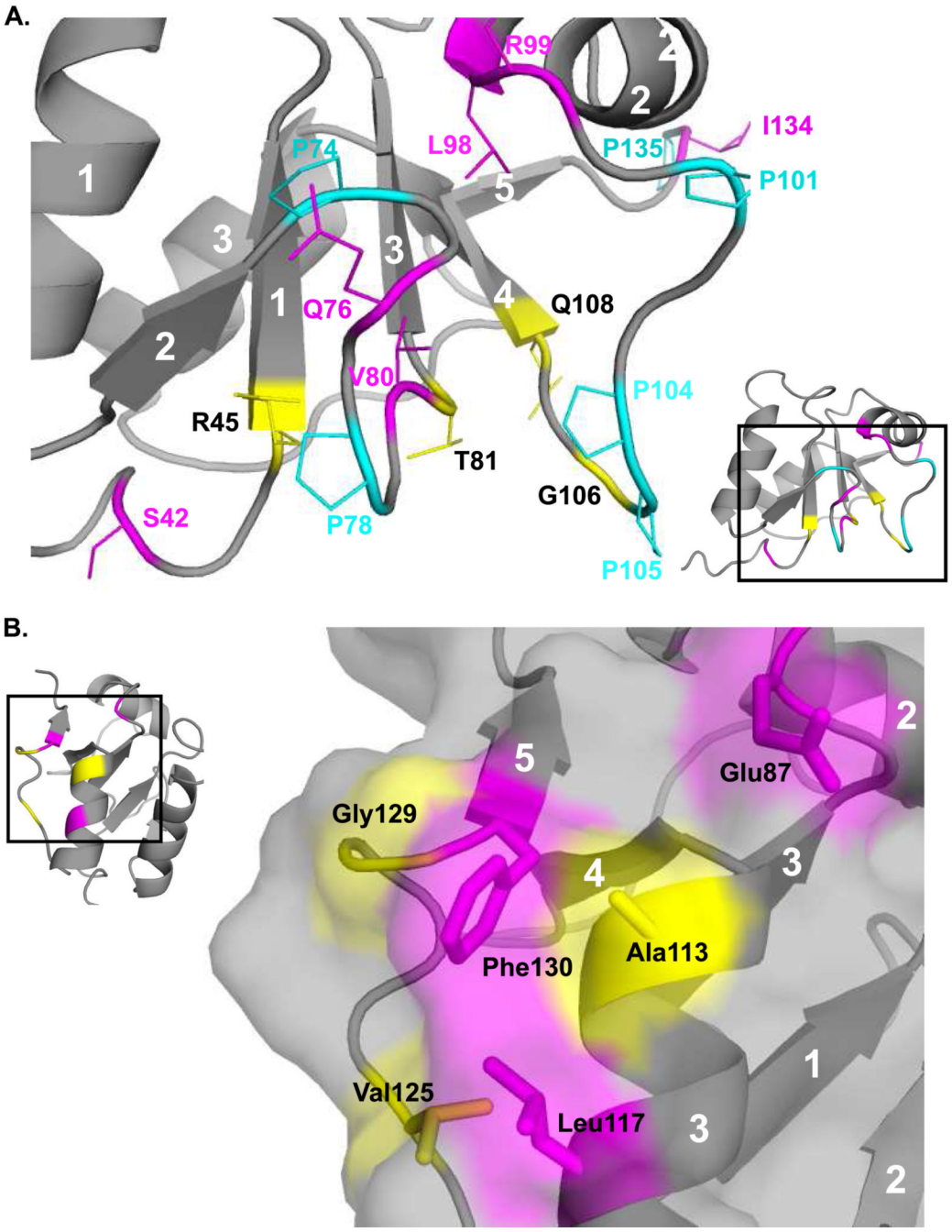

Figure 6.

Two views of slow motions in Pol λ BRCT domain. Residues that demonstrated R_{ex} from CPMG experiments are colored magenta, and residues with multiple peaks in the ^{15}N-^{1}H HSQC are colored yellow. Proline residues are colored cyan. (A). Numerous residues in the vicinity of prolines that display either R_{ex} or slow exchange cross-peaks. (B). A patch of surface-exposed residues that are mostly hydrophobic, and also show either R_{ex} or slow exchange cross-peaks.

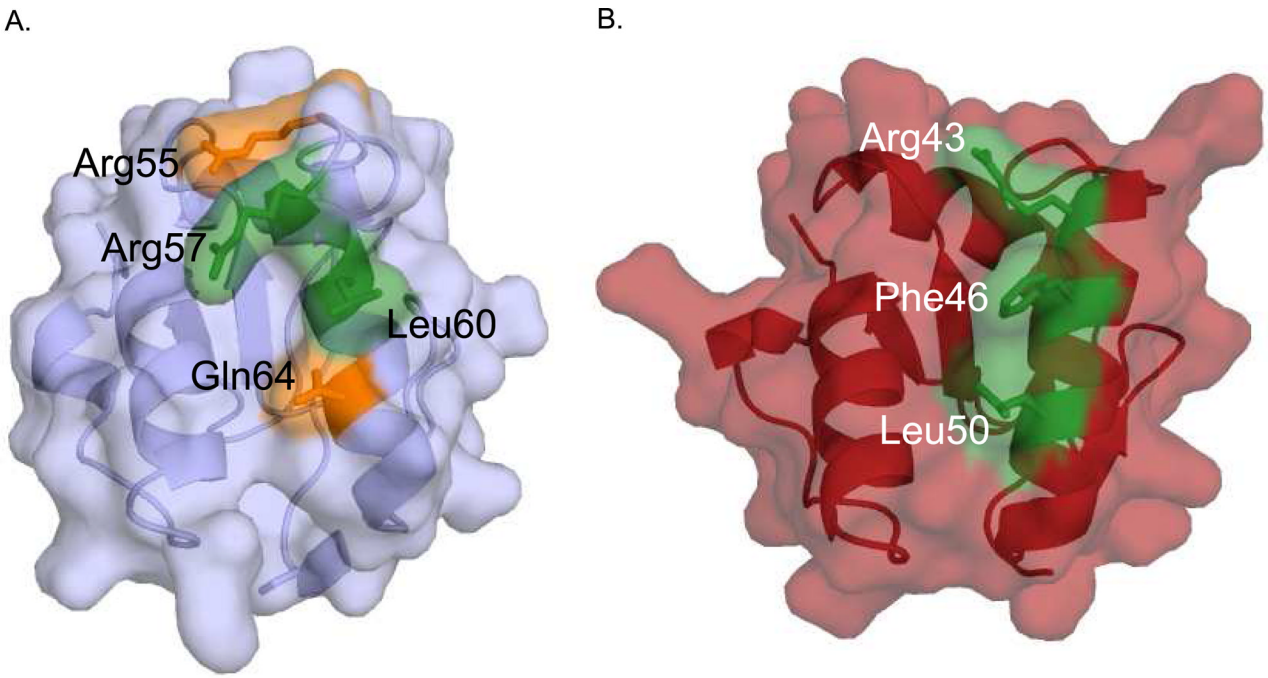

Figure 7.
Molecular surface of Pol λ and Pol μ BRCT domains, highlighting important residues for NHEJ interactions. Pol λ (A) and Pol μ (B) are rendered, highlighting residues tested for NHEJ activity. Residues with activity similar to wildtype are colored orange and residues showing decreased binding and NHEJ activity are colored green.

Table 1

Structural Statistics Summary

NOE distance restraints	
Intra-residue	396
Sequential	461
Medium range (*i*, *i*±2–4)	424
Long range (*i*, *i*>4)	635
Total	1916
HBDA (Hydrogen Bond Restraints)	32
Dihedral Restraints	115
RDC Restraints	37
Ensemble RMSD	
Secondary Structure Backbone	0.68
Secondary Structure Heavy	1.49
Violations	
NOE	2.5 +/− 1.1
RDC	0
Dihedral	0.67 +/− 0.65
RMS experimental	
NOE	0.047 +/− 0.005
Dihedral	0.87 +/− 0.17
HBDA	0.022 +/0 0.004
RDC	0.1 Hz +/− 0.02
(R-Factor)	0.1% +/− 0.05
RMS covalent geometry	
Bonds	0.0049 +/− 0.00029
Angles	0.52 +/− 0.023
Impropers	0.43 +/− 0.028
Ramachandran Space[(a)]	
Most Favored Region	69.1%
Additionally Allowed Region	19.8%
Generously Allowed Region	8.6%
Disallowed Region	2.5%

All data calculated with XPLOR-NIH [33], except for (a) calculated with PROCHECK [48].